DOI: 10.1002/ejic.200600677

Pentacarbonyl[2-(2′-pyridyl)quinoxaline-κN^4]tungsten: A Combined Study of Its Conformational and Electronic Structure Based on Experimental and DFT-TDDFT Data

Christodoulos Makedonas,[a] Irene Veroni,[a] and Christiana A. Mitsopoulou*[a]

Keywords: Pentacarbonyl complexes / 2-(2-Pyridyl)quinoxaline / Tungsten / DFT calculations / TD-DFT calculations / Pi stacking

Photolysis of $W(CO)_6$ in the presence of 2-(2′-pyridyl)quinoxaline (pq) results in the formation of $W(CO)_4$(pq) via an intermediate product $W(CO)_5(N^4$-pq) (**1**). In **1** the pq ligand that has three nitrogen atoms – two pyridine and one quinoxaline type – is coordinated in a monodentate fashion. This is the first example, where the pq ligand is coordinated in a monodentate fashion and especially from a quinoxaline nitrogen atom (N^4). Complex **1** has been fully characterized and its crystal structure has unambiguously demonstrated that pq is preferably coordinated through N^4 rather than the N^1 and $N^{1'}$ atoms, while its packing is governed by π–π interactions and hydrogen bonds. The almost perfect "face-to-face" alignment of the condensed quinoxaline rings is attributed to the existence of the electron-withdrawing groups, namely $W(CO)_5$ and the pyridine ring. The aforementioned preference for N^4 atoms has been elucidated by thermodynamic means and explained in terms of the frontier orbitals. Time-dependent density functional theory has been used for the investigation of the excited states of **1**. The calculated vertical excitation energies are consistent with the experimental data showing that the low-lying solvatochromic band of **1** in the UV/Vis spectra is best described by the term MLCT/LLCT.

1. Introduction

Both the photochemical substitution of complexes such as $M(CO)_6$ and the organometallic complexes between transition-metal carbonyls and N-containing heterocycles continues to be the subject of intense interest.[1] The photochemical and electronic properties, along with the potential of these complexes in industrial applications, have led to many studies for use as photosensitizers, catalysts, and conducting coordinating polymers.[2–4] Photolysis of the group VI metal hexacarbonyl compounds in the presence of potentially bidentate diimine-type ligands N–N [2,2′-bipyridines, 1,4-diazabutadienes, or 2-(2′-pyridyl)quinoxaline] ultimately results in the formation of the respective $M(CO)_4$(N–N) chelate complexes.[1,5–6] This process reportedly involves the initial photosubstitution of one CO group, leading to an intermediate product of type $M(CO)_5$(N–N) in which the N–N ligand is coordinated in a monodentate fashion. The importance of asymmetrical transition-metal complexes, namely $M(CO)_5L$ where M = Cr, W and L = π-conjugated ligand, in the field of second-order NLO materials is now very well documented.[7]

Among the aforementioned bidentate N–N ligands our attention has been attracted by 2-(2′-pyridyl)quinoxaline (pq), which combines the bridging properties of quinoxalines along with the chelating efficiency of 2,2′-bipyridine. The former can be explained by the discovery that polypyridyl ligands, which own low-lying LUMOs and contain more than one nucleophilic center, play an important role in the synthesis of metallo–organic compounds with various applications in material chemistry. Besides, the quinoxaline structure is widely recognized as an important component of a great number of natural compounds with applications in areas as diverse as antibacterial, antiviral, anticancer, antifungal, antihelmintic, insecticidal agents,[8] electron-withdrawing groups in p-conjugated polymer chemistry,[9] fluorescent dyes,[10,11] and optical-based sensors for anions in organic media.[12] While the vast majority of these materials are based on organic molecules there has been a growing interest in developing metal–containing compounds over the last few years. The central motivation behind this effort has been to combine the unique properties of transition-metal complexes (e.g. color, redox behavior) with those associated with the existence of the two nitrogen atoms in suitable bridging *para* positions, which can easily be functionalized allowing one to tailor their properties.[13]

[a] Inorganic Chemistry Laboratory, Department of Chemistry, National and Kapodistrian University of Athens, Panepistimiopolis, Zografou 15771, Greece
Fax: +30-210-8322828
E-mail: cmitsop@chem.uoa.gr

Up until now, a plethora of metal complexes have been reported where pq is bicoordinated through the N^1 and $N^{1'}$ atoms,[5,6,14,15] but there has never been any undoubted proof for coordination of a metal at a N^4 atom. In spite of this semi-empirical calculations have shown that the HOMO of pq is mostly a "lone" electron pair on N^1 and N^4,[16] thus these two nitrogen atoms should share almost the same propensity for coordination. The thermodynamic stability that offers the chelation of pq after its coordination at N^1 should be the major reason for the above experimental observation.

During the photolysis of $W(CO)_6$ in THF in the presence of pq we surprisingly discovered that the photogenarated ring closure reaction of $W(CO)_4$(pq) goes through $W(CO)_5$(N^4-pq) (**1**);[17] the latter has been isolated and fully characterized. In order to explain the preference of the N^4 atom over the N^1 and $N^{1'}$ atom upon ligation (Scheme 1), and explain the electronic spectra of **1**, we have undertaken a DFT and TDDFT study and combined the data with the experimental results.

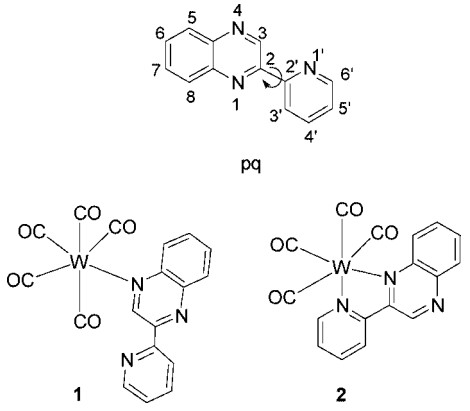

Scheme 1.

The main part of this report is organized as follows: in Section 2.1 a discussion of experimental data such as 2D NMR spectra indicating the coordinating nitrogen atom and crystal packing of **1** on the basis of the developed intermolecular forces is given. The theoretical results are critically analyzed and compared with experimental data in Section 2.2. This section is subdivided into two subsections. In the first subsection the ground state of **1** along with the structure of the other two possible isomers are discussed in terms of DFT data compared with the experimental structures. In the second part the predominant conformation structure is given in thermodynamic terms. Finally, in the last section, the UV/Vis spectrum is fully characterized by TD-DFT means.

2. Results and Discussion

2.1. NMR Spectroscopic Data and Crystal Packing

The complex $W(CO)_5$(pq) (**1**) is an intermediate product from the photolysis of $W(CO)_6$ in THF in the presence of pq leading to the photogenerated ring closure reaction $W(CO)_4$(pq). Surprisingly, the coordinated nitrogen atom is N^4 and not the usually referenced N^1. Of course, **1** is not the only intermediate product but it is the main one (yield 70%). The $W(CO)_5$(N^4-pq) (**1**) complex was isolated photochemically by a two-stage reaction (Scheme 2).

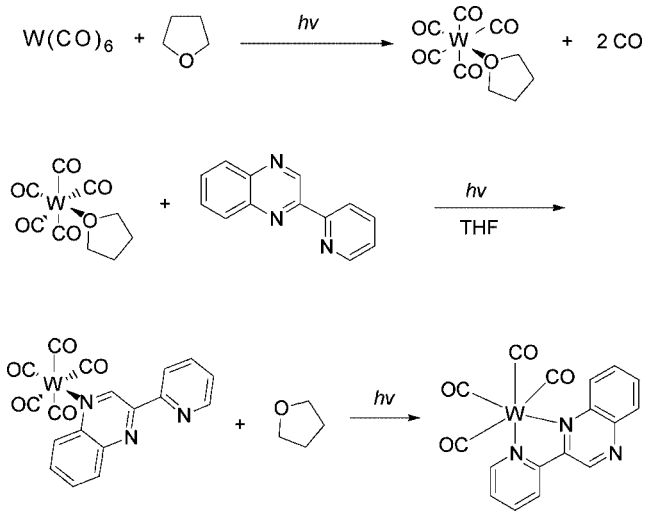

Scheme 2.

On the basis of a method by Strohmeier and Müller[18] the photolysis of $W(CO)_6$ in THF yields the mononuclear THF adduct $W(CO)_5$(THF), which on further photochemical reaction with an excess of pq after a short irradiation time (about 10 min) gives **1** as an orange solid in good yield; further irradiation yields **2**.

A first indication of the coordination site is provided by both ^{1}H NMR and HMBC ^{1}H-^{15}N NMR spectra of **1**. The HMBC ^{1}H-^{15}N NMR spectrum of pq in $CDCl_3$ (Figure 1) was considered as a first probe for the partial charges on the nitrogen atoms of the free ligand that could be extrapolated so as to provide us with the necessary evidences for the coordinated nitrogen atom in **1**. The aforementioned spectrum contains three independent *J* networks, where each nitrogen atom couples across two or three bonds with the adjacent protons. The nitrogen atoms are of the pyridine type, that is, they provide only one 2p electron to the involved π-electron system and they have their lone pairs in the plane of the conjugated system, in this way keeping their basicity. This is illustrated by the positions of the ^{15}N NMR chemical shifts that are characteristic of sp^2 hybridized nitrogen atoms.[19] Unfortunately, N^1 and N^4 cannot be assigned unequivocally as the long-range connectivity of both N^1 and N^4 with H^3 and correspondingly with H^8 and H^5 are not particularly enlightening since H^8 and H^5 are NMR equivalent. Nevertheless, it has been reported that the chemical shift of N^4 is relatively insensitive to the different heteroaromatic substituents at the 2-position of the quinoxaline ring,[20] while the ^{15}N NMR chemical shift of N^1 is found to be strongly dependent on these substituents. On this basis, the most downfield shifted nitrogen atom is N^4 (δ = 331 ppm), followed by N^1 (δ = 319 ppm) and $N^{1'}$ (δ = 311 ppm), this is in accordance with the semi-empirically calculated partial charges on the nitrogen atom

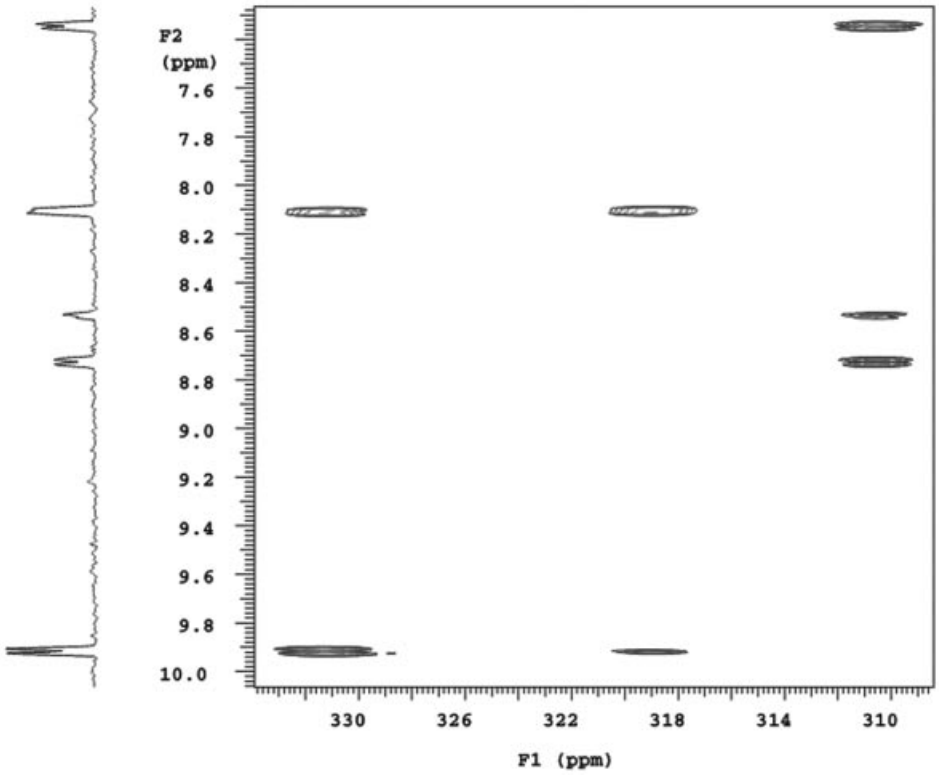

Figure 1. HMBC ^{1}H-^{15}N NMR spectra of **1**.

of pq.[19] The planarity of pq should establish an inter-annular conjugation between its quinoxaline and pyridyl moiety that allows the π-deficient quinoxaline moiety to accept π electron density from the pyridyl ring. This is illustrated by the downfield shift (deshielding) of the pyridine N in pq, in comparison to the ^{15}N NMR chemical shift in the (2-methyl)pyridine molecule.[19]

The ligation of pq to the $W(CO)_5$ moiety through the N^4 atom has been proven unambiguously by the elucidation of its structure by single-crystal X-ray diffraction methods.[17] Complex **1** crystallizes in the $P2_1/c$ space group. It is stacked in two different columns in a V-type assembly. In Figure 2, the crystal packing of the complex is depicted along the a axis. In each column the individual molecules are stacked in a "face-to-face" arrangement creating couples (Figure 3). The intermolecular distance of the N-ligand atoms (or planes) involved in this couple is 3.37 Å, suggesting π stacking with strong π–π interactions. Moreover, an almost perfect "face-to-face" alignment of the quinoxaline rings is observed, which is extremely rare.[21] This might be

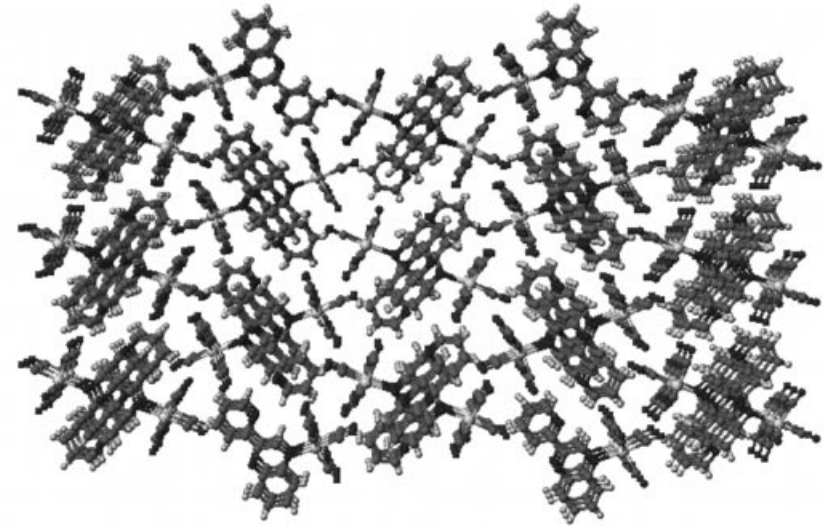

Figure 2. Crystal packing of **1** as it is viewed along the a axis.

because of the existence of the two electron-withdrawing groups present on the same quinoxaline ring, namely the $W(CO)_5$ fragment and the pyridine moiety, which cause a decrease in π-electron density on the parent ring and consequently the π–π repulsion. The aforementioned observations are of fundamental importance for the further development of inorganic supramolecular chemistry and the tuning and prediction of crystal structures. Moreover, an interesting feature observed in the crystal structure of **1** is the existence of two internal hydrogen bonds $H^{3'}$–N^2 [2.548 (0.060) Å and C–H···N = 101.59 (4.10)°] and H^3–N^1 [2.453 (0.54) Å and C–H···N = 103.37 (4.90)°] and two intermolecular hydrogen bonds between H atoms of the pq ligand and CO groups [H^5–O_{tr} 2.382(0.054) Å and 132.12 (4.63)° and H^8–O^4 2.514 (0.060) Å and 164.01 (5.18)°], which probably reflects their stacking.

Figure 3. π–π Interactions in complex **1**. A "face-to-face" alignment of quinoxaline rings that overlap with their nitrogen–carbon atoms.

2.2. Ground-State Structure

2-(2′-Pyridyl)quinoxaline with its three nitrogen atoms can adopt three different conformations when acting as a monodentate ligand to the $W(CO)_5$ fragment. The first conformation arises from ligation through the pyridine N^1, giving structure **N1**, the second arises from ligation through the $N^{1'}$ atom of the first quinoxaline, giving structure **N2**, whereas the third conformation leads to complex **1**, through ligation to **N4**, as pictorially depicted in Figure 4. During the photolytic procedure the parent compound $W(CO)_6$ reacts with the ligand in order to first afford the title complex. In the following sections, its ground-state and electronic behavior are studied by means of DFT calculations.

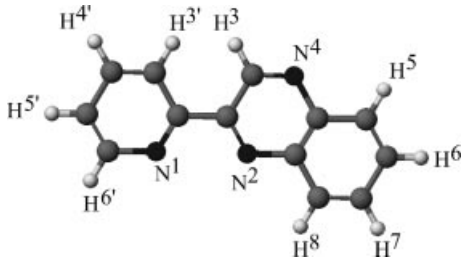

Figure 4. The three different coordination sites of the 2-(2′-pyridyl)quinoxaline ligand along with the numbering system of the H atoms.

2.2.1. Calculation of the Ground-State Structure

In $W(CO)_5$(pq) the tungsten has a distorted octahedral coordination sphere, as is expected, with the diimine ligand to adopt an *anti* conformation. DFT calculations were performed on complex **1** in the gas phase starting from crystallographic data. The main structural features that were taken from both the crystal structure **1** and the calculation **N4** are summarized in Table 1. In the same table structural characteristics of the other two possible isomers are also depicted (vide infra). All theoretical structures under study are viewed in a manner such that the coordinated nitrogen ligand (e.g. the quinoxaline in **N4**) bisects the $W(CO)_4$ fragment, while the noncoordinating nitrogen (e.g. the pyridine in **N4**) lies at the back side of the molecule. In this scheme the numbering of the equatorial carbonyls starts from the front right site of the molecule and continues clockwise. According to data presented in Table 1 the overall agreement between the theoretical (**N4**) and experimental (**1**) structures is generally satisfactory. Nevertheless, the geometrical features (distances and angles) associated with carbonyls 1 and 2 do not follow the general trend. The difference in W–C–O angles, along with the followed numbering scheme, is depicted in Figure 5.

Optimization of the molecule has been performed without any symmetry constraints. This, along with the successful application of the same combination of functional/core potential/basis set in the completely relevant case of the $W(CO)_4$(pq) complex[6] where the 2-(2′-pyridyl)quinoxaline acts as a bidentate ligand through N^1 and N^2, lead us to hypothesize that electronic effects on their own are not enough to cause carbonyls 1 and 2 to bend by at least 5° more than that of the carbonyls 3 and 4. In order to clarify this difference an inspection of the crystal structure of **1** is essential.

As we have already mentioned the packing of **1** in the solid state is governed by π–π interactions and hydrogen bonding. In Table 2 all the observed C–H···O short contacts are depicted. The entries printed in **bold** refer to the hydrogen bonds that we already mentioned (vide supra), two more entries shown printed in regular font type represent strong interactions, while six short contacts are also given in *italics*.

Both π-stacking and hydrogen bonding stabilize couples of molecules within the same column. Moreover, hydrogen bonds determine the final conformation of **1** within the $P2_1/c$ space group. We believe that the existence of these hydrogen bonds reflects the aforementioned structural differences between **1** and **N4**. In the case where the bonding scheme of CO^1 was exactly the same as that of CO^4 (88.6° for the N–W–C angle and 176.9° for the W–C–O angle) a decrease in the CO^1–$H^{4'}$ interaction (from 2.63 Å and 130.4° to 2.16 Å and 118.8°) and consequently the strengthening of the second short contact (CO^1–$H^{3'}$, from 3.03 Å and 130.4° to 2.46 Å and 106.2°) will occur. As a result the parent molecule will take a new position closest to the neighboring one and this could destabilize the packing. Taking into consideration the fact that, for electronic

Table 1. A comparison of the calculated selected bond lengths [Å] and angles [°] for the three different structural isomers with the experimental values **1** from the X-ray analysis.

C.I.	$W(CO)_5(pq)$			
M	**1**	**N4**	**N1**	**N2**
W–N	2.311(4)	2.321	2.360	2.408
$W–C_{trans}$	1.959(5)	1.987	1.984	1.977
W–C1	2.049(5)	2.037	2.041	2.037
W–C2	2.048(5)	2.037	2.032	2.033
W–C3	2.047(5)	2.040	2.038	2.037
W–C4	2.043(5)	2.040	2.041	2.056
$C–O_{trans}$	1.156(6)	1.188	1.188	1.189
C–O1	1.138(6)	1.183	1.182	1.185
C–O2	1.146(6)	1.183	1.186	1.184
C–O3	1.136(6)	1.182	1.182	1.184
C–O4	1.140(6)	1.182	1.183	1.179
$N–W–C_{tr}$	175.62(19)	177.5	176.1	176.6
N–W–C1	98.90(17)	93.5	85.9	95.5
N–W–C2	96.98(17)	93.5	92.2	88.5
N–W–C3	89.72(18)	89.4	93.5	93.2
N–W–C4	88.61(17)	89.4	96.0	95.6
$W–C–O_{tr}$	178.6(5)	180.0	179.8	179.5
W–C–O1	171.3(4)	176.9	179.0	174.3
W–C–O2	172.3(5)	176.9	175.7	176.9
W–C–O3	176.3(5)	177.7	177.9	173.2
W–C–O4	176.9(4)	177.7	173.8	171.7

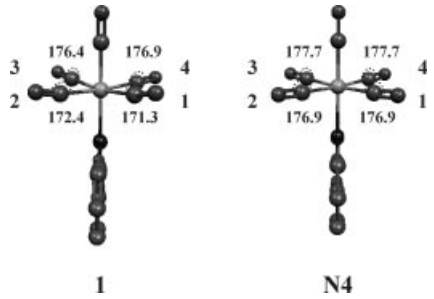

Figure 5. Differences in W–C–O angles between the theoretical (**N4**) and experimental (**1**) data.

Table 2. C–H···O short contacts in the crystal. *d* is the O···H distance in Å, φ is the C–H···O angle in °, X is the hydrogen nucleus and P the molecular column where it belongs to; S the same, N neighboring, V neighboring with a V conformation.

CO	*d*	φ	X	P
trans	**2.371**	**132.4**	**H5**	**V**
	2.837	*115.2*	*H6*	*V*
1	2.626	130.4	H4′	S
	3.029	*112.1*	*H3′*	*S*
2	*2.774*	*148.1*	*H3′*	*S*
3	*2.882*	*150.7*	*H6*	*N*
	3.036	*122.5*	*H8*	*S*
	3.172	*122.2*	*H7*	*S*
4	**2.517**	**164.1**	**H8**	**S**
	2.591	131.0	H5′	N

reasons, carbonyl coordination must be equal in couples (1–2 and 3–4) we conclude that the difference in binding angles arises in order for the stacking to be energetically more favorable.

On the basis of both experimental and theoretical results there are some points that certainly deserve to be further analyzed. Firstly, as it has already been mentioned (vide supra), tungsten has a distorted octahedral coordination sphere, and both the bonds W–N and $W–C_{tr}$ are almost equal to the relative bond lengths W–N(qn) and W–C11 (*trans* to the coordinated nitrogen atom) in $W(CO)_4(pq)$.[6] This implies a similar bonding behavior of the quinoxaline part of the ligand whatever the coordinated nitrogen atom. The induced *trans* influence from the N-donor is postulated by the W–C and C–O distances on the equatiorial plane. The $W–C_{tr}$ bond length is shorter than the relative distances in the equatorial plane, whereas the $C–O_{tr}$ bond is elongated. Secondly, the characteristic bending of carbonyls observed in several other carbonyl compounds is also present here.

To further discuss the aforementioned trend the orbital energies along with the contributions from the different ligands and the metal are given in Table 3. According to data presented in Table 3 the three highest occupied molecular orbitals of **N4** are close in energy and predominantly consist of metal d orbitals [d_{xz} in HOMO, d_{yz} in HOMO–1 and d_{z^2} (as a linear combination with $d_{x^2-y^2}$) in HOMO–2] with a significant contribution from the carbonyl π* orbitals.

These three orbitals are related to the t_{2g} orbital set in $W(CO)_6$[6,22] regarding their π*-back-bonding character. They are mainly dominated by π-type W–C bonding and C–O antibonding interactions and are indicative of the W→CO π* back-bonding. In the HOMO–2 these interactions are mainly localized on the equatorial plane, while in HOMO and HOMO–1 the contribution of the axial carbonyl group is ca. 12.8%. On the other hand, the orbitals HOMO–3 to HOMO–5 are localized on the quinoxaline moiety of the organic ligand; more precisely, HOMO–3 is

Table 3. Selected orbital energies and orbital compositions for the three conformations **N1**, **N2**, and **N4**. The HOMO and LUMO are shown in bold.

MO	*E* [eV]	W	CO^1	CO^2	CO^3	CO^4	CO_{tr}	qn	py
N1									
101	–1.78	8.6	30.1	12.7	29.5	12.9	0.4	0.7	5.1
100	–1.93	1.5	1.3	5.5	1.8	4.7	0.2	30.4	54.7
99	–2.14	9.1	14.3	6.5	10.1	7.8	0.5	23.5	28.2
98	–2.44	12.1	9.7	11.7	12.4	9.2	–0.3	8.1	37.2
97	**–2.91**	**1.6**	**0.6**	**1.4**	**0.1**	**1.4**	**0.9**	**67.4**	**26.6**
96	**–6.22**	**60.8**	**6.5**	**4.8**	**6.8**	**4.4**	**13.0**	**2.1**	**1.5**
95	–6.25	60.3	3.8	8.3	4.5	7.5	12.6	0.4	2.6
94	–6.66	60.5	9.6	9.9	9.3	9.2	0.0	1.1	0.4
93	–7.19	0.3	0.0	0.0	0.1	0.1	0.1	97.0	2.3
92	–7.26	0.1	0.0	0.0	0.0	0.1	0.0	97.1	2.7
91	–7.72	1.5	0.1	0.1	0.3	0.9	0.1	82.7	14.2
N2									
101	–1.65	4.5	14.9	2.2	14.8	2.2	0.8	15.1	45.6
100	–1.78	6.9	23.3	18.1	18.5	18.1	0.0	10.6	4.4
99	–2.03	6.1	1.8	12.8	1.4	11.8	–0.6	38.6	28.1
98	–2.23	13.8	20.0	8.4	22.0	7.2	–0.9	11.8	17.7
97	**–3.30**	**1.0**	**0.4**	**0.3**	**0.1**	**0.4**	**1.0**	**89.9**	**6.9**
96	**–6.09**	**61.1**	**3.1**	**8.5**	**3.8**	**6.8**	**13.9**	**1.0**	**2.0**
95	–6.21	59.1	9.7	3.2	8.7	2.9	12.4	3.6	0.3
94	–6.53	60.7	9.7	10.2	9.6	8.2	0.1	0.6	1.0
93	–7.61	0.5	0.1	0.1	0.0	1.0	0.1	55.7	42.5
92	–7.68	1.8	0.1	0.1	0.1	2.0	0.2	49.4	46.3
91	–7.85	0.6	0.1	0.1	0.4	0.1	0.2	60.1	38.7
N4									
101	–1.73	11.1	21.2	21.3	22.2	22.3	1.3	0.6	0.0
100	–1.80	9.0	22.9	22.9	21.1	21.1	0.5	2.1	0.5
99	–2.31	20.8	19.6	19.6	20.3	20.3	–1.5	1.0	0.1
98	–2.33	0.6	0.8	0.8	1.8	1.8	0.1	61.0	33.1
97	**–3.34**	**0.9**	**0.4**	**0.4**	**0.3**	**0.3**	**1.1**	**86.7**	**10.0**
96	**–6.24**	**59.3**	**5.6**	**6.1**	**5.2**	**5.3**	**12.4**	**5.7**	**0.0**
95	–6.25	63.0	5.8	5.7	5.8	5.7	13.2	0.8	0.1
94	–6.67	61.1	9.8	9.8	9.5	9.5	0.0	0.4	0.1
93	–7.37	0.6	0.0	0.0	0.0	0.0	0.1	57.5	41.6
92	–7.55	0.8	0.1	0.1	0.0	0.0	0.2	19.0	79.8
91	–7.86	0.7	0.0	0.0	0.2	0.2	0.1	87.8	11.0

delocalized over the three rings of the ligand, whereas HOMO–4 and HOMO–5 are localized mainly on the pyridine and quinoxaline moiety, respectively. The LUMO and LUMO+1 are dominated by quinoxaline π* orbitals of the ligand, whereas LUMO+2 to LUMO+4, also of π* character, arise mainly from the equatorial carbonyls. The HOMO and LUMO of **N4** are depicted in Figure 6.

An unoccupied orbital with a predominant d(σ*) character was not found among the spectroscopically important orbitals. In cases where this sort of contribution exists it corresponds to only a part of a highly delocalized orbital. Thus, low lying LF states, contradictory to the arguments of the traditional ligand field theory, are not expected. This is consistent with previous work done by Vlček et al.[23–27]

2.2.2. Conformational Analysis

Complex **1** can adopt three conformations in space as has already been mentioned. These conformations are depicted in Figure 7 and their structural characteristics are presented in Table 1.

The plane formed by the binding organic ring lies in an *anti* conformation to the $W(CO)_4$ fragment in **N4** with a C^3–N–W–$C_{(CO^3)}$ dihedral angle of 45.3°. This is more or less the same case for **N2** with a dihedral angle of 34.4°. On the contrary, in **N1** a *gauche* conformation is adopted, since the dihedral angle is 83.0°. The aforementioned difference for **N1** has a great impact on the structure, since the orthogonality holds only for the first coordination sphere around the central metal. Thus, the pyridine ligand bends away from the CO^3 moeity and the observed $C^{6'}$–N–W–C_{tr} dihedral angle is 45.7°. In other words, the structure is folded. But the most important structural difference between **N4** and **N1** and **N2** is that all the three aromatic rings of the ligand adopt a coplanar conformation in **N4**, but not in **N1** and **N2**. More specifically, a N^1–$C^{2'}$–C^2–N^2 dihedral angle of 127.5° and 64.4° is observed in **N1** and **N2**, respectively, in accordance with the one observed in the free ligand. This twisting around the single bond C^2–$C^{2'}$ is necessary for the system, otherwise if a coplanar arrangement was adopted there would be strong intramolecular interactions between

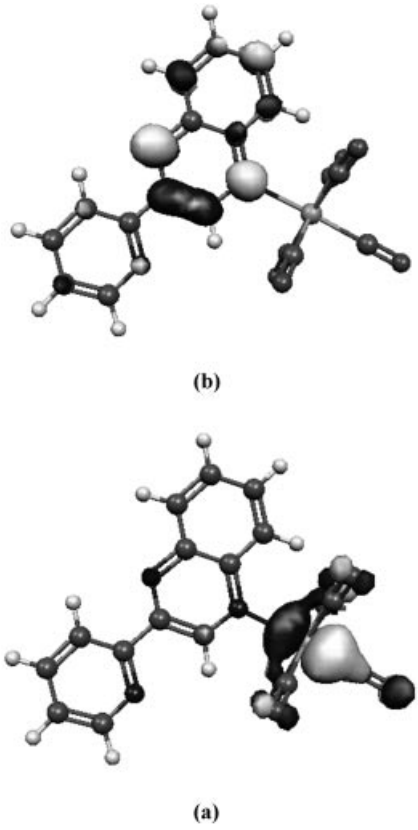

Figure 6. 0.05 a.u. contour plots of the HOMO (a) and LUMO (b) of complex **N4**.

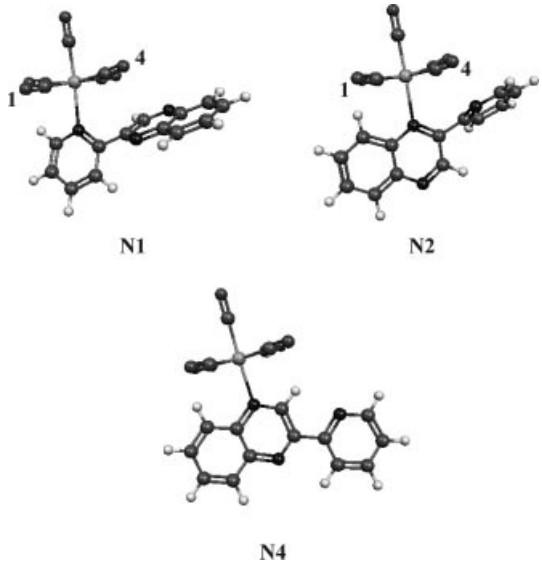

Figure 7. The three different conformations of the $W(CO)_4$(pq) complex. In the case of **N1** and **N2** the numbering of the carbonyls in front is also presented.

the noncoordinating organic ring and carbonyls 3 and 4. The W–N–C angles, as presented in Table 1, are indicative of these interactions. Thus, the values of the W–N–$C_{(CO^3)}$ [and W–N–$C_{(CO^4)}$] are larger than the relative values for W–N–$C_{(CO^1)}$ [and W–N–$C_{(CO^2)}$].

During the photolytic route to the $W(CO)_4$pq chelate ring closure, complex **1**, having the conformation **N4**, is the main intermediate product. In order to better understand this result, we performed a conformational analysis of the three isomers under study. Our results are summarized in Figure 8.

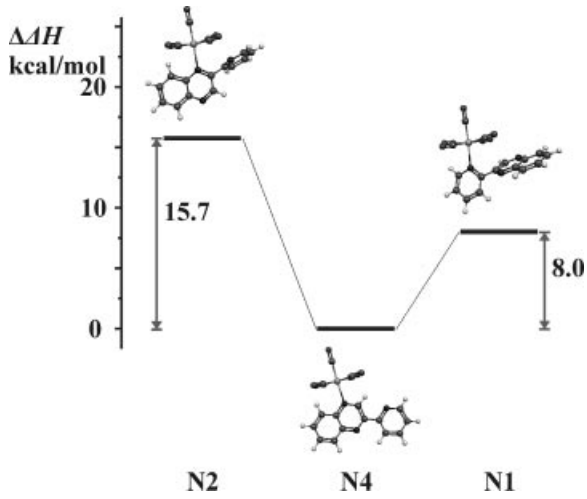

Figure 8. Energy differences among the conformations under study.

According to data presented in Figure 8, we concluded that the isomer **N4** has the most stable structure among the three conformational isomers. It is more stable by 8.0 kcal/mol than **N1** and by 15.7 kcal/mol than **N2**. The latter seems to be the less favorable isomer to be formed in the reaction process. The calculated difference in the stability of the isomers is attributed to electronic and steric repulsions between carbonyls 3 and 4 and the noncoordinating organic ring. In Figure 9, the three isomers are depicted using the space-filling model. The destabilization of the conformations **N1** and **N2** may attribute to the intramolecular $O_{(CO^4)}$–N interaction; the latter is not present in **N4**. More specifically, the $O_{(CO^4)}$–N^1 distance is 3.04 Å in **N2**, while in **N1** the $O_{(CO^4)}$–N2 and $O_{(CO^4)}$–N^4 distances are 3.38 Å and 3.53 Å, respectively.

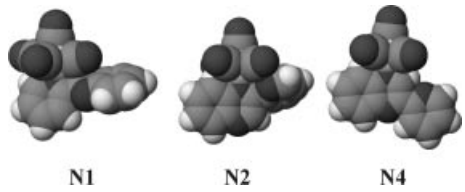

Figure 9. The structure of the three isomers with the space-filling model.

From an orbital point of view (Table 3 and Figure 10), we observe that the HOMO to HOMO–2, having a significant d_π-metal character, are destabilized in **N2** as compared with **N1** and **N4**. Moreover, an orbital inversion occurs. The HOMO of **N4**, mainly of a d_{xz}/π^*(CO) character of **N4** becomes HOMO–1 in the other two isomers. This inversion

happens since the HOMO–1 in **N4**, which contains a large contribution from the metal d_{yz} orbital, is destabilized from the presence of the twisted organic ring and becomes HOMO in **N1** and **N2**. Taking into consideration that tungsten-centered d_{xz} and d_{xy} orbitals in **1** are nearly degenerate the geometrical changes predicted in conformations **N1** to **N4** can cause intercrossing of the HOMO and HOMO–1. A nonextensive delocalization of electron cloud on the carbonyls in the HOMO and HOMO–1 has its origin in the presence of the twisted rings in **N1** and **N2** conformations. Thus, in **N4** the electron cloud is equipartitioned on the equatorial carbonyls; the situation is different in the case of the isomers **N1** and **N2**, with the asymmetry being more obvious in **N2**. This is another reason for the increase in the HOMO energy in the latter case. Moreover, in **N4** the diimine accepts more electron density from the $W(CO)_5$ core, through back-donation, as compared with **N1** and **N2**. This is postulated by the contributions of the coordinated organic ring to the HOMO in **N4** and to the HOMO–1 in the other two isomers. Finally, there is a substantial difference in the LUMO of the three isomers. In both **N2** and **N4** the LUMO is mainly localized on the coordinating ring of the ligand. On the contrary, in **N1** the contribution of the orbitals of the noncoordinated quinoxaline moiety to the LUMO is double that of the contribution of the coordinated pyridine ring. This reflects a significant increase in the energy of the **N1** LUMO, which becomes less stable. The HOMO and LUMO of conformations **N1** and **N2** are depicted in Figure 11 and Figure 12, respectively.

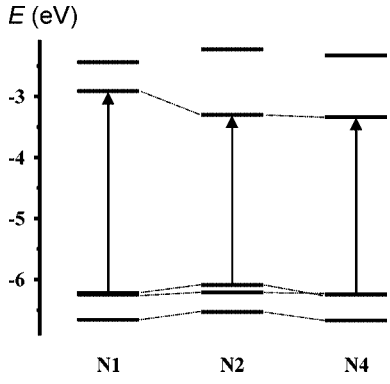

Figure 10. Energy diagram of the frontier orbitals of the three conformations under study.

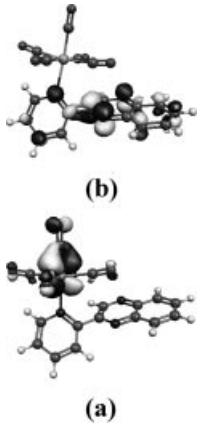

Figure 11. 0.05 a.u. contour plots of the HOMO (a) and LUMO (b) of complex **N1**.

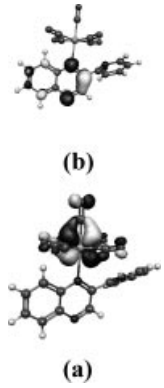

Figure 12. 0.05 a.u. contour plots of the HOMO (a) and LUMO (b) of complex **N2**.

2.3. Electronic Transitions and Excited States

The electronic absorption spectra of **1** in two solvents are indicated in Figure 13 and the corresponding data are included in Table 4. As a whole the spectra consist of three main bands: a broad and structured high-energy band extending from 309 to 380 nm, a shoulder at 398 nm, and a broad low-energy band. The change of the solvent mainly affects the low-energy band that is blue-shifted as the polarity of the solvent increases (negative solvatochromism).

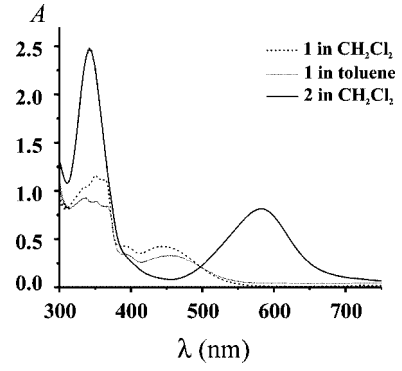

Figure 13. UV/Vis spectra of **1** and **2** in toluene and dichloromethane.

The shape along with the position and the solvent dependence of the low-energy band denote its (W)$d_\pi \rightarrow \pi^*$(L) charge-transfer (MLCT) character, which agrees with previous interpretations of many mononuclear metal pentacarbonyl complexes.[28] In order to investigate the lowest-lying singlet states of **1**, TDDFT calculations have been performed. Selected calculated low-lying singlet states along

Table 4. Position of the low-energy MLCT band of **1** in various solvents.

Solvents	λ_{max} [nm]
CCl_4	483
CH_2Cl_2	446
$CHCl_3$	455
$(CH_3CH_2)_2O$	449
C_6H_{14}	486
Toluene	459
THF	424

with their vertical excitation energies and oscillator strengths are displayed in Table 5. The transitions under study fulfill the criteria posed by Casida.[29]

The lowest in energy, highly solvatochromic transition of **1** can be assigned predominantly to the HOMO→LUMO ($n \rightarrow \pi^*$) transition since the contributions from several other transitions to the final state are minor. It is observed at 483 nm in CCl_4 and 455 nm in $CHCl_3$ and has W/CO → pq character. The fact that ca. 40% of the HOMO electron density is localized on parts of the molecule other than the metal (Table 3) contradicts the widely accepted MLCT notation for this transition; it could be characterized as an oversimplification. Therefore, we adopted the term MLCT/LLCT, suggested by Vlček and coworkers,[30] and employed it for the characterization of excited states of the relevant compound $W(CO)_4$(pq).[6] In the literature two other relative notations exist and can also be employed in our case. These are metal-ligand-to-ligand charge transfers (MLLCT)[31] and mixed-metal-ligand-to-ligand charge transfers (MMLL′CT).[32] The aforementioned transition arises from orbitals in total accordance with the case of the complex $W(CO)_5$(pyCN) described by Vlček and coworkers.[23] The shoulder of the main band on the high energy side, computed around 405 nm, is attributed to a superposition of several transitions with close energies and mainly to two MLCT(CO_{eq}) transitions of W/CO→CO_{eq} character. Finally, the higher-intensity broad band centered at 351 nm presenting a triple splitting and computed around 344 nm is mainly attributed to a double π–π*(pq) transition of the HOMO–3/HOMO–5 → LUMO character and a transition of MLCT/LLCT character. The MO picture given here is totally inconsistent with the traditional view that contains low-lying LF transitions. All calculated valence orbitals that contain metal contribution are highly delocalized. Thus no orbital of net d_{σ^*} character has been found with relatively low energy. So transitions with a predominant d–d charac-

Table 5. Selected TDDFT calculated energies and compositions of the lowest-lying singlet energy states together with oscillator strengths of **1**.[a] Only transitions with *f* greater than 0.001 are presented.

State	Composition[b]	ΔE[c]	*f*[d]	Character
3	**HOMO→LUMO**, ***92%***	**2.39**	**0.1049**	**W/CO→qn/py (MLCT/LLCT)**
5	HOMO–1→LUMO+2, *81%* HOMO–2→LUMO+4, *13%*	3.05	0.0080	W/CO→CO_{eq} (MLCT/LLCT)
6	HOMO→LUMO+2, *80%* HOMO–2→LUMO+3, *13%*	3.06	0.0104	W/CO→CO_{eq} (MLCT)
9	HOMO→LUMO+1, *69%* HOMO–2→LUMO+2, *18%* HOMO→LUMO+3, *6%*	3.28	0.0031	W/CO→qn/py (MLCT/LLCT)
12	HOMO→LUMO+3, *48%* HOMO–1→LUMO+4, *23%* HOMO→LUMO+1, *14%* HOMO–2→LUMO+2, *13%*	3.38	0.0036	W/CO→CO_{eq} (MLCT) W/CO→CO_{eq} (MLCT) W/CO→qn/py (MLCT/LLCT) W/CO_{eq}→qn/py (MLCT/LLCT)
14	HOMO–1→LUMO+4, *67%* HOMO→LUMO+3, *31%*	3.50	0.0070	W/CO→CO_{eq} (MLCT)
15	HOMO-3→LUMO, *81%*	3.61	0.1338	π–π*(pq)
19	HOMO→LUMO+6, *32%* HOMO→LUMO+5, *25%* HOMO–2→LUMO+4, *25%* HOMO–5→LUMO, *14%*	3.83	0.0046	W/CO_{eq}→qn/py (MLCT/LLCT)
20	HOMO–5→LUMO, *67%* HOMO–3→LUMO+1, *7%* HOMO–2→LUMO+4, *6%* HOMO→LUMO+5, *5%*	3.90	0.0460	π–π*(pq)

[a] The principal singlet transition responsible for the main absorption band in the visible region is shown in **bold**. [b] Compositions of electronic transitions are expressed in terms of contributing excitations between ground-state Kohn–Sham molecular orbitals. [c] Transition energy from the a^1S ground state in eV. [d] Oscillator strength.

ter are not expected to be observed in the UV/Vis spectra of **1**. In Figure 13, the UV/Vis spectrum of $W(CO)_4(pq)$[6] (**2**) in CH_2Cl_2 is also presented. Bidentate coordination of the pq ligand, with the simultaneous abstraction of the CO moiety, induces several optical effects. The most important is that the main solvatochromic W/CO → qn/py transition exhibits a strong red shift (≈0.66 eV), because of the destabilization of the orbitals localized on carbonyl ligands. The latter is a consequence of the chelation of pq that results in a less efficient back-donation from the metal to the carbonyls. Thus, the optically active HOMO in **1**, which also reflects the back-donation to the N-ligand becomes HOMO–2 in **2** (ΔE = 0.34 eV). Moreover, if we consider that CO_{tr} of **1** is analogous to CO_{eq} of **2** then HOMO–1 and HOMO–2 in **1** become HOMO (ΔE = 0.74 eV) and HOMO–1 (ΔE = 0.91 eV) in **2**, respectively. On the other hand, the LUMO and LUMO+1, localized on pq, are stabilized in **2** as the pq contribution is increased from 10% in **1** to 25% in **2**. On the other hand, the ligand based π–π* transitions are kept almost constant in both complexes as depicted in Figure 13. Finally, comparing the molar absorptivities of both complexes (1600 $M^{-1}cm^{-1}$ for **1** and 3600 $M^{-1}cm^{-1}$ for **2**) we observe that they are in total accordance with the oscillator strengths, where *f* is 0.1049 (Table 5) and 0.1158[5] for **1** and **2**, respectively. The larger oscillator strength of **2** can be related to a better overlap between the contributed orbitals of the transition. In other words, a better overlap among the orbitals of pq and the $W(CO)_4$ fragment is obtained when the pq is coordinated in a bidentate fashion as in **2** compared with a monodentate one as in **1**.

3. Conclusions

The isolation of the monodentate intermediate $W(CO)_5$-(N^4-pq) (**1**), en route to photolytic $W(CO)_4$(pq) chelate ring closure has been achieved. This is the first example where the ligand pq is coordinated in a monodentate fashion. Complex **1** has been fully characterized and its crystal structure has unambiguously demonstrated that pq is preferably coordinated through N^4 rather than the N^1 and N^2 atoms, while its packing is governed by π–π interactions and hydrogen bonds. The face-to-face alignment of condensed quinoxaline rings is attributed to the existence of the electron-withdrawing groups, namely $W(CO)_5$ and the pyridine ring.

The aforementioned preference for the N^4 atom has been elucidated both by theoretical (structural and thermodynamic) means and in terms of the frontier orbitals. The theoretical calculations reveal that the coplanarity of the pq ligand, which exists in the **N4** conformation in accordance with the experimental results, no longer exists in the **N1** and **N2** conformations. Actually, the coordinated pyridine moiety of the ligand to the $W(CO)_5$ fragment in **N1**, keeping a *gauche* conformation, causes a twist and fold of the whole pq molecule; whereas the same ring in **N2**, which is noncoordinated, is twisted along the C^2–$C^{2'}$ bond. This results in a destabilization of the electronic distribution as is indicated by the energies of the frontier orbitals and leads to new intramolecular interactions. This situation is best described by DFT thermodynamic calculations. Thus, it is predicted that the **N4** conformation should be more stable than the other two conformations (8.0 kcal/mol vs. **N1** and 15.7 kcal/mol vs. **N2**).

Moreover, the ground state of **1** has been fully elucidated by DFT means. Thus, the HOMO and HOMO–1 of **1** are nearly degenerate and predominantly consist of tungsten 5d orbitals with near equal contributions from quinoxaline and carbonyl ligands. The LUMO is energetically well separated and is practically a pure π* orbital localized on the quinoxaline moiety of the ligand. Finally, the electronic transitions of **1** have been fully characterized by TD-DFT calculations, indicating that its low lying solvatochromic band is best ascribed as a HOMO to LUMO transition. Since it has a W/CO → pq character the term MLCT/LLCT is adopted.

Experimental Section

Materials and Equipment: The ligand 2,2′-pq was synthesized as described previously.[5,6] The complex $W(CO)_6$ along with THF, which was used in the syntheses, were obtained from Aldrich Chemicals and used after being dried. The solvents used in UV/Visible spectroscopic studies were purified to spectroscopic quality by standard methods.[33] The deuterated solvents, which were utilized in the NMR spectroscopic experiments were purchased from Aldrich and were of 99.99% purity.

The photolysis experiment was carried out with a 1000 W Xenon lamp with an Oriel, model 68820, Universal Arc. Lamp source selected with an appropriate interference filter (Corning). FT-IR spectra in solution and with KBr pellets were recorded with a Nicolet Magna IR 560 spectrophotometer with a 1.0 cm^{-1} resolution. Electronic absorption spectra were recorded with a Varian Cary 300 spectrometer with a circulating thermostat. The solute concentration was about 10^{-5} M and the samples were prepared just before the measurements were taken. The ^1H-^{15}N HMBC NMR spectra were recorded with a Varian INOVA 500-MHz NMR spectrometer using NH_3 as the external standard. Microanalyses were performed with a Euro Vector EA 3000 analyzer

Synthesis of the $W(CO)_5(N^4$-pq) Complex 1: A tetrahydrofuran solution (50 mL) of the parent hexacarbonyltungsten (0.351 g, 1 mmol) was deoxygenated by continuous nitrogen purging and then irradiated with a 1000 W Xenon lamp at 25 °C for 20 min. An excess amount of pq (0.269 g, approximately 30%) was then added to the reaction vessel and the irradiation was continued for 10 more minutes. The tetrahydrofuran was slowly evaporated under atmospheric pressure and the residue was passed through a silica gel column using hexane as the eluent. After slow evaporation of the hexane, complex **1** was obtained as an orange solid in 70% (0.372 g) yield. $C_{18}H_9N_3O_5W$ (531.12): calcd. C 40.60, H 1.72, N 7.91, O, 15.12, W 34.81; found C 40.70, H 1.71, N 7.89, O 15.00. IR (in DCM): $\tilde{\nu}_{CO}$ = 2073 (w), 1932 (st), 1904 (m) cm^{-1}.

Computational Details: Ground-state electronic structure calculations of all compounds under investigation have been performed using density functional theory (DFT)[34] methods employing the GAUSSIAN 2003 software package.[35] The functional that was used throughout this study is the B3LYP, consisting of a hybrid exchange functional as defined by Becke's three-parameter equa-

tion[36] and the Lee–Yang–Parr correlation functional.[37] The ground-state geometries were obtained in the gas phase by full geometry optimization starting from structural data. The optimum structures located as stationary points on the potential energy surfaces were verified by the absence of imaginary frequencies. The derived wave functions were found free from internal instabilities. The basis set used throughout this study is the full double-ζ LANL2DZ basis functions along with the corresponding effective core potential for tungsten.[38] The thermodynamic data given in this report include zero-point energy (ZPE) and thermal corrections, without the introduction of scaling factors. Percentage compositions of molecular orbitals from the contributing fragments (the central metal, the diimine, and the axial and equatorial carbonyls) were calculated and analyzed using the AOMix and AOMix-S progams.[39] The first 21 singlet excited states of the closed shell complex were calculated within the TDDFT formalism.[40] The percentage of different transitions contributing to a state and the simulations of calculated IR spectra, when needed, were calculated with the aid of SWizard.[41] The graphics presented in the report have been prepared with the aid of the Molekel[42] and CAChe[43] programs.

Acknowledgments

The project was cofunded by the European Social Fund (EPEAEK II)and National Resources (PYTHAGORAS). We also thank the Special Research Account of NKUA.

[1] D. J. Stufkens, *Coord. Chem. Rev.* **1990**, *104*, 39–112.
[2] C. A. Hunter, *Angew. Chem. Int. Ed. Engl.* **1995**, *34*, 1079–1081.
[3] P. J. Stang, D. H. Cao, S. Saito, A. M. Arif, *J. Am. Chem. Soc.* **1995**, *117*, 6273–6283 and references cited therein.
[4] I. Y. Wu, J. T. Lin, J. Luo, S. S. Sun, C. S. Li, K. J. Lin, C. Tsai, C. C. Hsu, J. L. Lin, *Organometallics* **1997**, *16*, 2038–2048.
[5] I. Veroni, A. Rontoyianni, C. A. Mitsopoulou, *Dalton Trans.* **2003**, 255–260.
[6] I. Veroni, C. Makedonas, A. Rontoyianni, C. A. Mitsopoulou, *J. Organomet. Chem.* **2006**, *691*, 267–281.
[7] M. Bruschi, P. Fantucci, M. Pizzotti, *J. Phys. Chem. A* **2005**, *109*, 9637–9645.
[8] B. Zarranz, A. Jaso, I. Aldana, A. Monge, *Bioorg. Med. Chem.* **2004**, *12*, 3711–3721.
[9] M. X. Chen, E. Perzon, N. Robisson, S. K. M. Jönsson, M. R. Andersson, M. Fahlman, M. Berggren, *Synth. Met.* **2004**, *146*, 233–236.
[10] D. W. Rangnekar, N. D. Sonawane, *Dyes Pigm.* **2000**, *45*, 87–96.
[11] A. Katoh, T. Yoshida, J. Ohkanda, *Heterocycles* **2000**, *52*, 911–920.
[12] S. V. Shevchuk, V. M. Lynch, J. L. Sessler, *Tetrahedron* **2004**, *60*, 11283–11291 and references cited therein.
[13] W. Kaim, *Angew. Chem. Int. Ed. Engl.* **1983**, *22*, 171–190.
[14] C.-X. Shao, W.-H. Sun, Z.-L. Li, Y.-L. Hu, L.-Q. Han, *Catal. Commun.* **2002**, *3*, 405–410.
[15] A. Garoufis, A. Koutsodimou, N. Katsaros, C. A. Mitsopoulou, N. Hadjiliadis, *Polyhedron* **1999**, *18*, 361–369.
[16] E. G. Bakalbassis, J. Mrozinski, S. P. Perlepes, N. Hadjiliadis, F. Lianza, A. Albinati, *Polyhedron* **1994**, *13*, 3209–3218.
[17] I. Veroni, C. A. Mitsopoulou, F. J. Lahoz, *J. Organomet. Chem.* **2006**, submitted.
[18] W. Strohmeier, F. J. Müller, *Chem. Ber.* **1969**, *102*, 3608–3612.
[19] M. Witanowski, L. Stefaniak, G. A. Webb, *Nitrogen NMR Spectroscopy*, Annual Reports on NMR Spectroscopy, Academic Press, London, **1986**, *18*, p. 1.
[20] L. Hilfert, G. Sarodnick, G. Kempter, E. Kleinpeter, *J. Mol. Struct.* **1998**, *444*, 199–211.
[21] C. Janiak, *J. Chem. Soc., Dalton Trans.* **2000**, 3885–3896.
[22] A. Rosa, E. J. Baerends, S. J. A. van Gisbergen, E. van Lenthe, J. A. Goeneveld, J. G. Snijders, *J. Am. Chem. Soc.* **1999**, *121*, 10356–10365.
[23] S. Záliš, M. Busby, T. Kotrba, P. Matousek, M. Towrie, A. Vlček Jr., *Inorg. Chem.* **2004**, *43*, 1723–1734 and references cited therein.
[24] S. Záliš, I. R. Farrel, A. Vlček Jr., *J. Am. Chem. Soc.* **2003**, *125*, 4580–4592.
[25] I. R. Farrel, H. František, S. Záliš, T. Mahabiersing, A. Vlček Jr., *J. Chem. Soc., Dalton Trans.* **2000**, 4323–4331.
[26] I. R. Farrel, J. van Slageren, S. Záliš, A. Vlček Jr., *Inorg. Chim. Acta* **2001**, *315*, 44–52.
[27] S. Záliš, A. Vlček Jr., C. Daniel, *Collect. Czech. Chem. Commun.* **2003**, *68*, 89–104.
[28] A. Hameed, A. Rybarczyk-Pirek, J. Zakrzewski, *J. Organomet. Chem.* **2002**, *656*, 102–107.
[29] M. E. Casida, C. Jamorski, K. C. Casida, D. R. Salahub, *J. Chem. Phys.* **1998**, *108*, 4439–4449.
[30] I. R. Farrel, A. Vlček Jr., *Coord. Chem. Rev.* **2000**, *208*, 87–101.
[31] a) A. B. Tamayo, S. Garon, T. Sajoto, P. I. Djurovich, I. M. Tsyba, R. Bau, M. E. Thompson, *Inorg. Chem.* **2005**, *44*, 8723–8732; b) J. M. Villegas, S. R. Stoyanov, W. Huang, D. P. Rillema, *Inorg. Chem.* **2005**, *44*, 2297–2309; c) J. M. Villegas, S. R. Stoyanov, J. H. Reibensies, D. P. Rillema, *Organometallics* **2005**, *24*, 395–404; d) S. R. Stoyanov, J. M. Villegas, A. J. Cruz, L. L. Lockyear, J. H. Reibensies, D. P. Rillema, *J. Chem. Theory Comput.* **2005**, *1*, 95–106; e) J. M. Villegas, S. R. Stoyanov, W. Huang, L. L. Lockyear, J. H. Reibensies, D. P. Rillema, *Inorg. Chem.* **2004**, *43*, 6383–6396; f) S. Kar, B. Sarkar, S. Ghumaan, D. Roy, F. A. Urbanos, J. Fiedler, R. B. Sunoj, R. Jimenez-Aparicio, W. Kaim, G. K. Lahiri, *Inorg. Chem.* **2005**, *44*, 8715–8722.
[32] a) C. Makedonas, C. A. Mitsopoulou, *Eur. J. Inorg. Chem.* **2006**, 2460–2468; b) C. Makedonas, C. A. Mitsopoulou, *Eur. J. Inorg. Chem.* **2006**, 590–598; c) C. Makedonas, C. A. Mitsopoulou, *Spectrochim. Acta Part A* **2006**, *64*, 918–930; d) C. Makedonas, C. A. Mitsopoulou, F. J. Lahoz, A. I. Balana, *Inorg. Chem.* **2003**, *43*, 8853–8865.
[33] D. D. Perrin, W. L. F. Armarego, *Purification of Laboratory Chemicals*, Pergamon Press, 3rd ed., **1988**.
[34] R. G. Parr, W. Yang, *Density Functional Theory of Atoms and Molecules*, Oxford University Press, Oxford, **1989**.
[35] M. J. Frisch, G. W. Trucks, H. B. Schlegel, G. E. Scuseria, M. A. Robb, J. R. Cheeseman, J. A. Montgomery Jr., T. Vreven, K. N. Kudin, J. C. Burant, J. M. Millam, S. S. Iyengar, J. Tomasi, V. Barone, B. Mennucci, M. Cossi, G. Scalmani, N. Rega, G. A. Petersson, H. Nakatsuji, M. Hada, M. Ehara, K. Toyota, R. Fukuda, J. Hasegawa, M. Ishida, T. Nakajima, Y. Honda, O. Kitao, H. Nakai, M. Klene, X. Li, J. E. Knox, H. P. Hratchian, J. B. Cross, C. Adamo, J. Jaramillo, R. Gomperts, R. E. Stratmann, O. Yazyev, A. J. Austin, R. Cammi, C. Pomelli, J. W. Ochterski, P. Y. Ayala, K. Morokuma, G. A. Voth, P. Salvador, J. J. Dannenberg, V. G. Zakrzewski, S. Dapprich, A. D. Daniels, M. C. Strain, O. Farkas, D. K. Malick, A. D. Rabuck, K. Raghavachari, J. B. Foresman, J. V. Ortiz, Q. Cui, A. G. Baboul, S. Clifford, J. Cioslowski, B. B. Stefanov, G. Liu, A. Liashenko, P. Piskorz, I. Komaromi, R. L. Martin, D. J. Fox, T. Keith, M. A. Al-Laham, C. Y. Peng, A. Nanayakkara, M. Challacombe, P. M. W. Gill, B. Johnson, W. Chen, M. W. Wong, C. Gonzalez, J. A. Pople, *Gaussian 03, Revision B.1*, Gaussian, Inc., Pittsburgh PA, **2003**.
[36] A. D. Becke, *J. Chem. Phys.* **1993**, *98*, 5648–5652.
[37] C. Lee, W. Yang, R. G. Parr, *Phys. Rev. B* **1988**, *37*, 785–789.
[38] a) T. H. Dunning Jr., P. J. Hay, in: *Modern Theoretical Chemistry* (Ed.: H. F. Schaefer III), Plenum Press, New York, **1976**, vol. 3; b) P. J. Hay, W. R. Wadt, *J. Chem. Phys.* **1985**, *82*, 270–283.

[39] a) S. I. Gorelsky, *AOMix and AOMix-S progam, revision 6.11*, http://www.sg-chem.net/; b) S. I. Gorelsky, A. B. P. Lever, *J. Organomet. Chem.* **2001**, *635*, 187–196.
[40] R. Stratmann, G. Scuseria, M. Frisch, *J. Chem. Phys.* **1998**, *109*, 8218–8224.
[41] S. I. Gorelsky, *SWizard progam*, http://www.sg-chem.net/.
[42] P. Flükiger, H. P. Lüthi, S. Portman, J. Weber, *MOLEKEL Version 4.3*, Swiss Center for Scientific Computing, Manno, Switzerland, **2000–2002**.
[43] CAChe Worksystem 4.4, Fujitsu Ltd., **2000**.

Received: July 19, 2006
Published Online: November 6, 2006

